Chapter 4

Triangular Shell Elements.

An important advantage of the co-rotational formulation is the "reuse" of existing linear finite elements for large-rotation small-strain analysis. Chapters 4 and 5 develop high-performance shell elements that can efficiently provide the internal forces $\mathbf{f}_e$ and linear stiffness $\mathbf{K}_e$ used in the co-rotational nonlinear analysis presented in Chapters 2 and 3. The term "high performance" collectively identifies elements that can provide engineering accuracy with fairly coarse discretization.

Chapter 4 develops a triangular shell element whereas Chapter 5 develops a 4-node quadrilateral shell element. Both elements include drilling degrees of freedom as part of their membrane components.

In the exposition below, the special identifiers used in the previous chapters to distinguish linear and nonlinear components are dropped for clarity since the most of the development deals with the formulation of linear elements. Thus $\mathbf{K}_e$, for example, is written simply as $\mathbf{K}$.

4.1 Element stiffness by the ANDES formulation.

Let $\mathbf{K}$ denote the linear element stiffness matrix, $\mathbf{v}$ the visible element degrees of freedoms and $\mathbf{f}$ the corresponding element forces. The element stiffness equations for the elements developed below can be written as

$$\mathbf{K}\mathbf{v} = (\mathbf{K}_b + \mathbf{K}_h)\mathbf{v} = \mathbf{f} \ . \tag{4.1.1}$$

Here $\mathbf{K}_b$ and $\mathbf{K}_h$ are called *basic* and *higher-order* stiffness matrices respectively. This decomposition of the element stiffness equations also applies to the quadrilateral shell element constructed in the next chapter.

$\mathbf{K}_b$ is formulation independent in that it is entirely defined by an assumed constant stress together with an assumed boundary displacement field. This approach to forming the basic stiffness was first developed by Bergan and Hanssen [00] and later integrated in the the more developed form of the Free Formulation (FF) by Bergan and Nygård [00, 00].

$\mathbf{K}_h$ can be formed using several different formulations, most notably the FF, the Extended Free Formulation (EFF) [00] and the Assumed Natural Deviatoric Strains (ANDES) formulation. The latter grew out of work done by Felippa to incorporate FF into a variational framework [00, 00], combined with further developments by Militello and Felippa [00, 00].

4.1.1 Basic stiffness construction.

The procedure for constructing the basic stiffness can be found in several sources. Militello has a very enlightening description in his Ph.D thesis [00]. This step by step outline of the basic stiffness construction is also described in Reference [00], and is outlined below here for easy reference.

B1. Assume a constant stress state, $\bar{\boldsymbol{\sigma}}$ inside the element. This gives the associated boundary tractions $\bar{\boldsymbol{\sigma}}_n$:

$$\bar{\boldsymbol{\sigma}}_n = \bar{\boldsymbol{\sigma}} \cdot \mathbf{n} = \mathbf{T}_n \bar{\boldsymbol{\sigma}} \ , \tag{4.1.2}$$

where $\mathbf{n}$ is the outward unit normal vector on the element boundary and $\mathbf{T}_n$ is a transformation matrix that substitutes the tensor-product $\bar{\sigma_{ni}} = \bar{\sigma}_{ij} n_j$ with an equivalent matrix-multiply.

B2. Connect a boundary displacement field, $\mathbf{d}$, to the visible degrees of freedom, $\mathbf{v}$ as

$$\mathbf{d} = \mathbf{N}_d \mathbf{v} \ . \tag{4.1.3}$$

Matrix $\mathbf{N}_d$ contains boundary displacement functions that must satisfy inter-element continuity, and exactly include rigid body and constant strains motion. Note, however, that the internal displacement field need not be defined here at this point; and in fact in the ANDES formulation such field is not explicitly constructed.

B3. Construct the force-lumping matrix, $\mathbf{L}$, that consistently "lumps" the boundary tractions $\bar{\boldsymbol{\sigma}}_n$ to element node forces that are conjugate to the visible degrees of freedom $\mathbf{v}$ in the virtual work sense:

$$\int_S \delta \mathbf{d}^T \bar{\boldsymbol{\sigma}}_n dS = \int_S \delta \mathbf{v}^T \mathbf{N}_d^T \mathbf{T}_n \bar{\boldsymbol{\sigma}} dS = \delta \mathbf{v}^T \int_S \mathbf{N}_{dn}^T dS \, \bar{\boldsymbol{\sigma}} = \delta \mathbf{v}^T \mathbf{L} \bar{\boldsymbol{\sigma}} = \delta \mathbf{v}^T \bar{\mathbf{f}}. \tag{4.1.4}$$

This equation provides the lumping matrix $\mathbf{L}$ as

$$\mathbf{L} = \int_S \mathbf{N}_d^T \mathbf{T}_n dS = \int_S \mathbf{N}_{dn}^T dS \ . \tag{4.1.5}$$

B4. The basic stiffness is constructed as

$$\mathbf{K}_b = \frac{1}{V} \mathbf{L} \mathbf{C} \mathbf{L}^T \ , \tag{4.1.6}$$

where $\mathbf{C}$ is the stress-strain constitutive matrix, and V is the volume of a three-dimensional element. (V is replaced by area and length measures for two-dimensional and one-dimensional elements, respectively.)

4.1.2 Higher order stiffness by the ANDES formulation.

Militello gives a thorough description of the ANDES formulation in his Ph.D thesis [00] . This includes a point by point description of the construction of the higher order stiffness. This is also described by Felippa and Militello in [00] . The essence of this development outlined below is the use of assumed strain distribution, rather than displacement modes, to characterize the higher-order behavior of the element.

H1. Select locations in the element where "natural straingage" locations are to be chosen. For many ANDES elements these gages are placed on *reference lines* but this is not a general rule. By appropriate interpolation, express the element natural strains $\boldsymbol{\epsilon}$ in terms of the "straingage readings" at those locations:

$$\boldsymbol{\epsilon} = \mathbf{A}_\epsilon \mathbf{g} \,, \tag{4.1.7}$$

where $\boldsymbol{\epsilon}$ is a strain field in natural coordinates that must include all constant strain states. (For structural elements the term "strain" is to be interpreted in a generalized sense, for example curvatures for beams or plate bending elements.)

H2. Relate the Cartesian strains $\mathbf{e}$ to the natural strains:

$$\mathbf{e} = \mathbf{T}\boldsymbol{\epsilon} = \mathbf{T}\mathbf{A}_\epsilon \mathbf{g} = \mathbf{A}\mathbf{g} \tag{4.1.8}$$

at each point in the element. (If $\mathbf{e} \equiv \boldsymbol{\epsilon}$, or if it is possible to work throughout in natural coordinates, this step is skipped. This is often the case if $\mathbf{T}$ is constant over the element as for the triangular shell elements developed here.)

H3. Relate the natural straingage readings $\mathbf{g}$ to the visible degrees of freedom

$$\mathbf{g} = \mathbf{Q}\mathbf{v} \,, \tag{4.1.9}$$

where $\mathbf{Q}$ is a straingage-to-node displacement transformation matrix. Techniques for doing this vary from element to element and it is difficult to state rules that apply to every situation. Often this step is amenable to breakdown into subproblems; for example

$$\mathbf{g} = \mathbf{Q}_1\mathbf{v}_1 + \mathbf{Q}_2\mathbf{v}_2 + \ldots \tag{4.1.10}$$

where $\mathbf{v}_1$, $\mathbf{v}_2$, ... are conveniently selected subsets of $\mathbf{v}$. Some of these components may be derivable from displacements while others are not.

H4. Split the Cartesian strain field into mean (volume-averaged) and deviatoric strains:

$$\mathbf{e} = \bar{\mathbf{e}} + \mathbf{e}_d = (\bar{\mathbf{A}} + \mathbf{A}_d)\mathbf{g} \,, \tag{4.1.11}$$

where $\bar{\mathbf{A}} = \frac{1}{V}\int_V \mathbf{T}\mathbf{A}_\epsilon dV$, and $\mathbf{e}_d = \mathbf{A}_d\mathbf{g}$ has mean zero value over V. For elements with simple element geometry this decomposition can often be done in advance, and $\mathbf{e}_d$ constructed directly. Furthermore, this step may also be carried out on the natural strains if $\mathbf{T}$ is constant.

H5. The higher order stiffness matrix is given by

$$\mathbf{K}_h = \beta \mathbf{Q}^T \mathbf{K}_d \mathbf{Q} \,, \quad \text{with} \quad \mathbf{K}_d = \int_V \mathbf{A}_d^T \mathbf{C} \mathbf{A}_d \, dV \,, \tag{4.1.12}$$

where $\beta > 0$ is a scaling coefficient. It is often convenient to combine the product of $\mathbf{A}$ and $\mathbf{Q}$ into a single strain-displacement matrix called (as usual) $\mathbf{B}$, which splits into $\bar{\mathbf{B}}$ and $\mathbf{B}_d$:

$$\mathbf{e} = \mathbf{A}\mathbf{Q} = (\bar{\mathbf{A}} + \mathbf{A}_d)\mathbf{Q}\mathbf{v} = (\bar{\mathbf{B}} + \mathbf{B}_d)\mathbf{v} = \mathbf{B}\mathbf{v} \,, \tag{4.1.13}$$

in which case

$$\mathbf{K}_h = \beta \int_V \mathbf{B}_d^T \mathbf{C} \mathbf{B}_d \, dV \,. \tag{4.1.14}$$

We next apply these rules to the construction of a three-node triangular shell element. Because the element is flat, the membrane and bending can be developed separately. Both developments, however, share the geometric information presented in the following subsection.

4.2 Geometric definitions for a triangular element.

The geometry of a three-node triangular element is graphically defined in Figure 4.1.

By defining l_i to be length of side edge opposite to node i and h_i as height from node i to side i according to Figure 4.1 one obtains

$$l_i = \sqrt{x_{jk}^2 + y_{jk}^2} \qquad \text{and} \qquad h_i = \frac{2A}{l_i} \,, \tag{4.2.1}$$

where A is the triangle area, which may be calculated as

$$2A = x_{21}y_{31} - x_{31}y_{21} = x_{31}y_{12} - x_{12}y_{32} = x_{13}y_{23} - x_{23}y_{13} \,. \tag{4.2.2}$$

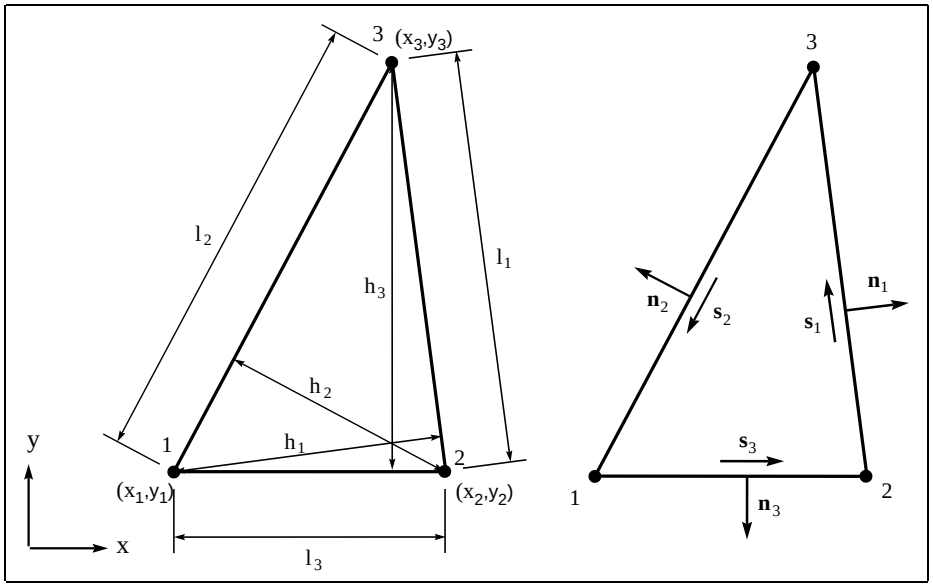

Figure 4.1. Geometric dimensions and unit vector definitions for a triangular element.

The unit vector $\mathbf{s}_i$ along side i and the outward normal vector $\mathbf{n}_i$ at side i can then be defined as

$$\mathbf{s}_i = \left\{ \begin{array}{c} s_{ix} \\ s_{iy} \\ 0 \end{array} \right\} = \frac{1}{l_i} \left\{ \begin{array}{c} x_{kj} \\ y_{kj} \\ 0 \end{array} \right\} \qquad \text{and} \qquad \mathbf{n}_i = \left\{ \begin{array}{c} n_{ix} \\ n_{iy} \\ 0 \end{array} \right\} = \left\{ \begin{array}{c} -s_{iy} \\ s_{ix} \\ 0 \end{array} \right\}. \tag{4.2.3}$$

4.3 The triangular membrane element.

The construction of an ANDES triangular membrane element is described by Felippa and Militello in [00]. The present description is adapted to the notation used for the four-node quadrilateral element in Chapter 5.

The nodal degrees of freedom $\mathbf{v}_i$ for the membrane element consists of the in-plane translations u, v and the "drilling" degree of freedom θ_z :

$$\mathbf{v}_i = \left\{ \begin{array}{c} u_i \\ v_i \\ \theta_{zi} \end{array} \right\}. \tag{4.3.1}$$

4.3.1 Basic stiffness.

The lumping of the constant membrane stresses to a node j is only a function of the neighboring side edges ij and jk. The total lumping matrix can thus be divided into the contributions to the separate nodes as

$$\mathbf{L} = \begin{bmatrix} \mathbf{L}_1 \\ \mathbf{L}_2 \\ \mathbf{L}_3 \end{bmatrix} , \tag{4.3.2}$$

where

$$\mathbf{L}_j = \frac{1}{2} \begin{bmatrix} y_{ki} & 0 & -x_{ki} \\ 0 & -x_{ki} & y_{ki} \\ \frac{\alpha}{6}(y_{ij}^2 - y_{kj}^2) & \frac{\alpha}{6}(x_{ij}^2 - x_{kj}^2) & \frac{\alpha}{3}(x_{kj}y_{kj} - x_{ij}y_{ij}) \end{bmatrix} , \tag{4.3.3}$$

and the nodal indices (i, j, k) take cyclic permutations of $(1, 2, 3)$. The basic stiffness is then computed as

$$\mathbf{K}_b = \frac{t}{A}\mathbf{L}\mathbf{C}\mathbf{L}^T , \tag{4.3.4}$$

where t is the element thickness and A the element area.

4.3.2 Higher order stiffness.

Felippa and Millitello [00] extracted the higher order behavior of the element by defining the higher order degrees of freedom $\tilde{\theta}_i$ as the nodal drilling degrees of freedom minus the rigid body and constant strain rotation θ_0 of the CST element

$$\tilde{\theta}_i = \theta_i - \theta_0 , \tag{4.3.5}$$

where

$$\theta_0 = \frac{1}{4A} [\, -x_{32} \quad -y_{32} \quad 0 \quad -x_{13} \quad -y_{13} \quad 0 \quad -x_{21} \quad -y_{21} \quad 0 \,] \, \mathbf{v} . \tag{4.3.6}$$

By further splitting the hierarchical rotations into mean $\bar{\theta} = (\tilde{\theta}_1 + \tilde{\theta}_2 + \tilde{\theta}_3)/3$ and deviatoric components $\theta'_i = \tilde{\theta}_i - \bar{\theta}$ one gets

$$\begin{Bmatrix} \theta'_1 \\ \theta'_2 \\ \theta'_3 \\ \bar{\theta} \end{Bmatrix} = \begin{bmatrix} 0 & 0 & \frac{2}{3} & 0 & 0 & -\frac{1}{3} & 0 & 0 & -\frac{1}{3} \\ 0 & 0 & -\frac{1}{3} & 0 & 0 & \frac{2}{3} & 0 & 0 & -\frac{1}{3} \\ 0 & 0 & -\frac{1}{3} & 0 & 0 & -\frac{1}{3} & 0 & 0 & \frac{2}{3} \\ \frac{x_{32}}{4A} & \frac{y_{32}}{4A} & \frac{1}{3} & \frac{x_{13}}{4A} & \frac{y_{13}}{4A} & \frac{1}{3} & \frac{x_{21}}{4A} & \frac{y_{21}}{4A} & \frac{1}{3} \end{bmatrix} \begin{Bmatrix} v_{x1} \\ v_{y1} \\ \theta_1 \\ v_{x2} \\ v_{y2} \\ \theta_2 \\ v_{x3} \\ v_{y3} \\ \theta_3 \end{Bmatrix} , \tag{4.3.7}$$

which in matrix form reads

$$\boldsymbol{\theta}_h = \mathbf{H}_{\theta v}\mathbf{v} \ . \tag{4.3.8}$$

The pure-bending field.
The pure bending field is connected to the deviatoric hierarchical rotations θ'_i as

$$\boldsymbol{\epsilon}_{b1} = \left\{ \begin{array}{c} \epsilon_{b21|1} \\ \epsilon_{b32|1} \\ \epsilon_{b13|1} \end{array} \right\} = \left[\begin{array}{ccc} \rho_1\chi_{21|1} & -\rho_2\chi_{21|1} & \rho_4\chi_{21|1} \\ \rho_5\chi_{32|1} & \rho_3\chi_{32|1} & -\rho_3\chi_{32|1} \\ -\rho_1\chi_{13|1} & \rho_4\chi_{13|1} & \rho_2\chi_{13|1} \end{array} \right] \left\{ \begin{array}{c} \theta'_1 \\ \theta'_2 \\ \theta'_3 \end{array} \right\} = \mathbf{Q}_{b1}\boldsymbol{\theta}'$$

$$\boldsymbol{\epsilon}_{b2} = \left\{ \begin{array}{c} \epsilon_{b21|2} \\ \epsilon_{b32|2} \\ \epsilon_{b13|2} \end{array} \right\} = \left[\begin{array}{ccc} \rho_2\chi_{21|2} & -\rho_1\chi_{21|2} & \rho_4\chi_{21|2} \\ \rho_4\chi_{32|2} & \rho_1\chi_{32|2} & -\rho_2\chi_{32|2} \\ -\rho_3\chi_{13|2} & \rho_5\chi_{13|2} & \rho_3\chi_{13|2} \end{array} \right] \left\{ \begin{array}{c} \theta'_1 \\ \theta'_2 \\ \theta'_3 \end{array} \right\} = \mathbf{Q}_{b2}\boldsymbol{\theta}'$$

$$\boldsymbol{\epsilon}_{b1} = \left\{ \begin{array}{c} \epsilon_{b21|3} \\ \epsilon_{b32|3} \\ \epsilon_{b13|3} \end{array} \right\} = \left[\begin{array}{ccc} \rho_3\chi_{21|3} & -\rho_3\chi_{21|3} & \rho_5\chi_{21|3} \\ \rho_4\chi_{32|3} & \rho_2\chi_{32|3} & -\rho_1\chi_{32|3} \\ -\rho_2\chi_{13|3} & \rho_4\chi_{13|3} & \rho_1\chi_{13|3} \end{array} \right] \left\{ \begin{array}{c} \theta'_1 \\ \theta'_2 \\ \theta'_3 \end{array} \right\} = \mathbf{Q}_{b3}\boldsymbol{\theta}' \tag{4.3.9}$$

where

$$\chi_{ij|k} = \frac{4A}{3l_{ij}^2} \quad \text{and} \quad \chi_{ij|i} = \chi_{ij|j} = -\frac{2A}{3l_{ij}^2} \tag{4.3.10}$$

and the ρ_i are numerical coefficients to be chosen. Coefficients ρ_i that optimize in-plane bending behavior of rectangular mesh units are found to be [00]

$$\rho_2 = 1 \ , \quad \rho_3 = \frac{1}{2} \quad \text{and} \quad \rho_1 = \rho_4 = \rho_5 = 0 \ . \tag{4.3.11}$$

Having defined the matrices $\mathbf{Q}_{bi}$ in (4.3.9), the bending strains over the element can now be interpolated linearly between the nodes:

$$\epsilon_b = (\zeta_1\mathbf{Q}_{b1} + \zeta_2\mathbf{Q}_{b2} + \zeta_2\mathbf{Q}_{b2})\boldsymbol{\theta}' = \mathbf{B}_b\boldsymbol{\theta}' \ . \tag{4.3.12}$$

The torsional field.
The torsional field is connected to the mean deviatoric rotation $\bar{\theta}$ and is given in [00] as

$$\epsilon_t = \left\{ \begin{array}{c} \epsilon_{t21} \\ \epsilon_{t32} \\ \epsilon_{t13} \end{array} \right\} = 3 \left\{ \begin{array}{c} \chi_{21|1}\zeta_{21} \\ \chi_{32|2}\zeta_{21} \\ \chi_{13|3}\zeta_{21} \end{array} \right\} \bar{\theta} = \mathbf{B}_t\bar{\boldsymbol{\theta}} \ .$$

The total strain field.

The total natural coordinate strain field is the combination of the pure-bending and torsional strain fields expressed with respect to the visible degrees of freedom

$$\begin{aligned}\boldsymbol{\epsilon} &= \boldsymbol{\epsilon}_b + \boldsymbol{\epsilon}_t \\ &= \mathbf{B}_b\boldsymbol{\theta}' + \mathbf{B}_t\bar{\theta} \\ &= [\,\mathbf{B}_b \quad \mathbf{B}_t\,]\,\boldsymbol{\theta}_h \\ &= [\,\mathbf{B}_b \quad \mathbf{B}_t\,]\,\mathbf{H}_{\theta v}\mathbf{v} \\ &= \mathbf{B}\mathbf{v}\ .\end{aligned} \tag{4.3.13}$$

The stiffness matrix.

The higher order stiffness matrix is computed as

$$\mathbf{K}_h = \int_A \mathbf{B}^T\mathbf{C}_\epsilon\mathbf{B}\,dA \quad \text{where} \quad \mathbf{C}_\epsilon = \mathbf{T}^T\mathbf{C}\mathbf{T}\ , \tag{4.3.14}$$

and

$$\mathbf{T}^{-1} = \begin{bmatrix} {s_{12}}_x^2 & {s_{12}}_y^2 & s_{12x}s_{12y} \\ {s_{23}}_x^2 & {s_{23}}_y^2 & s_{23x}s_{23y} \\ {s_{31}}_x^2 & {s_{31}}_y^2 & s_{31x}s_{31y} \end{bmatrix}. \tag{4.3.15}$$

Matrix $\mathbf{T}$ transforms the natural coordinate strains to Cartesian strains, while $\mathbf{T}^{-1}$ does the opposite.

4.4 The triangular bending elements.

The bending component of the triangular shell element is based on the linear three node plate bending element AQR developed by Militello [00]. A higher order stiffness is also developed by sanitizing the BCIZ element [00]. Two basic stiffnesses exist, one based on linear interpolation of normal rotations along a side edge and one based on quadratic variation of the normal rotation. The triangular ANDES bending elements can thus be formed by combining several basic and higher order stiffnesses.

The nodal bending degrees of freedom $\mathbf{v}_i$ consists of the out of plane translation w and the in-plane rotations θ_x and θ_y

$$\mathbf{v}_i = \begin{Bmatrix} w_i \\ \theta_{x\,i} \\ \theta_{x\,i} \end{Bmatrix}. \tag{4.4.1}$$

4.4.1 Basic stiffnesses.

$\mathbf{K}_b$ is one of the basic stiffness matrices described by Militello in [00] as

$$\mathbf{K}_b = \frac{1}{A}\mathbf{L}_l \mathbf{C} \mathbf{L}_l^T \quad \text{or} \quad \mathbf{K}_b = \frac{1}{A}\mathbf{L}_q \mathbf{C} \mathbf{L}_q^T \,,$$

where

$$\mathbf{L}_l = \begin{bmatrix} \mathbf{L}_{l1} \\ \mathbf{L}_{l2} \\ \mathbf{L}_{l3} \end{bmatrix} \quad \text{and} \quad \mathbf{L}_q = \begin{bmatrix} \mathbf{L}_{q1} \\ \mathbf{L}_{q2} \\ \mathbf{L}_{q3} \end{bmatrix} .$$

$\mathbf{L}_{q_i}$ and $\mathbf{L}_{q_i}$ are described in equation (0.0.0) and (0.0.0) respectively. The nodal indices (i, j, k) in the equations above takes the cyclic permutations of $(1, 2, 3)$ as in the case of the membrane lumping.

4.4.2 BCIZ higher order stiffness.

The BCIZ element developed by Bazeley et al. [00] is an historically important nonconforming element. However, the element is known not to pass the Patch Test. In fact the puzzling behavior of the element motivated the original development of that test. The use of the BCIZ element as an higher order stiffness for a triangular Free Formulation plate bending element was developed by Felippa, Haugen and Militello [00]. The transverse displacement field of the BCIZ element was given explicitly by Felippa [00] as

$$w = \left\{ \begin{array}{c} \zeta_1^2(3-2\zeta_1) + 2\zeta_1\zeta_2\zeta_3 \\ -\zeta_1^2(y_{12}\zeta_2 + y_{13}\zeta_3) - \frac{1}{2}(y_{12}+y_{13})\zeta_1\zeta_2\zeta_3 \\ \zeta_1^2(x_{12}\zeta_2 + x_{13}\zeta_3) + \frac{1}{2}(x_{12}+x_{13})\zeta_1\zeta_2\zeta_3 \\ \zeta_2^2(3-2\zeta_2) + 2\zeta_1\zeta_2\zeta_3 \\ -\zeta_2^2(y_{23}\zeta_3 + y_{21}\zeta_1) - \frac{1}{2}(y_{23}+y_{21})\zeta_1\zeta_2\zeta_3 \\ \zeta_2^2(x_{23}\zeta_3 + x_{21}\zeta_1) + \frac{1}{2}(x_{23}+x_{21})\zeta_1\zeta_2\zeta_3 \\ \zeta_3^2(3-2\zeta_3) + 2\zeta_1\zeta_2\zeta_3 \\ -\zeta_3^2(y_{31}\zeta_1 + y_{32}\zeta_2) - \frac{1}{2}(y_{31}+y_{32})\zeta_1\zeta_2\zeta_3 \\ \zeta_3^2(x_{31}\zeta_1 + x_{32}\zeta_2) + \frac{1}{2}(x_{31}+x_{32})\zeta_1\zeta_2\zeta_3 \end{array} \right\}^T \mathbf{v}$$

The strain displacement matrix $\mathbf{B}_\chi$ giving the natural curvatures from the visible degrees of freedom is obtained by double differentiation of the displacement field with respect to the triangular coordinates and appropriate relations detailed in the Appendix of [00]:

$$\boldsymbol{\chi} = \left\{ \begin{array}{c} \chi_{12} \\ \chi_{23} \\ \chi_{31} \end{array} \right\} = \mathbf{B}_\chi \mathbf{v} = (\mathbf{B}_{\chi 0} + \mathbf{B}_{\chi 1}\zeta_1 + \mathbf{B}_{\chi 2}\zeta_2 + \mathbf{B}_{\chi 3}\zeta_3)\mathbf{v} \,,$$

where

$$\mathbf{B}_{\chi 0}^T = \begin{bmatrix} 6 & 0 & 6 \\ 0 & 0 & 0 \\ 0 & 0 & 0 \\ 6 & 6 & 0 \\ 0 & 0 & 0 \\ 0 & 0 & 0 \\ 0 & 6 & 6 \\ 0 & 0 & 0 \\ 0 & 0 & 0 \end{bmatrix}, \quad \mathbf{B}_{\chi 1}^T = \begin{bmatrix} -12 & -4 & -12 \\ 4y_{12} & y_{12}+y_{13} & 4y_{13} \\ -4x_{12} & -x_{12}-x_{13} & -4x_{13} \\ 0 & -4 & 0 \\ -2y_{21} & -y_{21}+y_{23} & 0 \\ 2x_{21} & x_{21}-x_{23} & 0 \\ 0 & -4 & 0 \\ 0 & -y_{31}+y_{32} & -2y_{31} \\ 0 & x_{31}-x_{32} & 2x_{31} \end{bmatrix},$$

$$\mathbf{B}_{\chi 2}^T = \begin{bmatrix} 0 & 0 & -4 \\ -2y_{12} & 0 & -y_{12}+y_{13} \\ 2x_{12} & 0 & x_{12}-x_{13} \\ -12 & -12 & -4 \\ 4y_{21} & 4y_{23} & y_{21}+y_{23} \\ -4x_{21} & -4x_{23} & -x_{21}-x_{23} \\ 0 & 0 & -4 \\ 0 & -2y_{32} & y_{31}-y_{32} \\ 0 & 2x_{32} & -x_{31}+x_{32} \end{bmatrix},$$

and

$$\mathbf{B}_{\chi 3}^T = \begin{bmatrix} -4 & 0 & 0 \\ y_{12}-y_{13} & 0 & -2y_{13} \\ -x_{12}+x_{13} & 0 & 2x_{13} \\ -4 & 0 & 0 \\ y_{21}-y_{23} & -2y_{23} & 0 \\ -x_{21}+x_{23} & 2x_{23} & 0 \\ -4 & -12 & -12 \\ y_{31}+y_{32} & 4y_{32} & 4y_{31} \\ -x_{31}-x_{32} & -4x_{32} & -4x_{31} \end{bmatrix}.$$

By using a natural curvature constitutive matrix $\mathbf{C}_\chi = \mathbf{T}^T\mathbf{C}\mathbf{T}$ the higher order stiffness matrix becomes

$$\mathbf{K}_h = \int_A \mathbf{B}_{\chi d}^T \mathbf{C}_\chi \mathbf{B}_{\chi d}\, dA,$$

where $\mathbf{B}_{\chi_d} = \mathbf{B}_\chi - \bar{\mathbf{B}}_\chi$ and $\bar{\mathbf{B}}_\chi = \mathbf{B}_{\chi 0} + \frac{1}{3}(\mathbf{B}_{\chi 1} + \mathbf{B}_{\chi 2} + \mathbf{B}_{\chi 3})$.

4.4.3 ANDES higher order stiffness by direct curvature readings.

The three node ANDES element is based on direct curvature interpolation of the natural curvatures. As reference lines Millitello [00] chose the three side edges, which function as Hermitian beams. The nodal strain gage readings expressed as function of the visible degrees of freedom can be written

$$\mathbf{g} = \mathbf{Q}\mathbf{v} = \mathbf{Q}_F * \mathbf{F}\mathbf{v} \ , \tag{4.4.2}$$

where

$$\begin{aligned} \mathbf{g}^T &= [\, \kappa_{31|1} \quad \kappa_{12|1} \quad \kappa_{12|2} \quad \kappa_{23|2} \quad \kappa_{23|3} \quad \kappa_{31|3} \,], \\ \mathbf{v}^T &= [\, v_{z1} \quad \theta_{x1} \quad \theta_{y_1} \quad v_{z2} \quad \theta_{x2} \quad \theta_{y_2} \quad v_{z3} \quad \theta_{x3} \quad \theta_{y_3} \,], \end{aligned} \tag{4.4.3}$$

$$\mathbf{Q}_F = \begin{bmatrix} -6 & 4 & 4 & 0 & 0 & 0 & 6 & 2 & 2 \\ -6 & -4 & -4 & 6 & -2 & -2 & 0 & 0 & 0 \\ & & & & & & & & \\ 6 & 2 & 2 & -6 & 4 & 4 & 0 & 0 & 0 \\ 0 & 0 & 0 & -6 & -4 & -4 & 6 & -2 & -2 \\ & & & & & & & & \\ 0 & 0 & 0 & 6 & 2 & 2 & -6 & 4 & 4 \\ 6 & -2 & -2 & 0 & 0 & 0 & -6 & -4 & -4 \end{bmatrix} \tag{4.4.4}$$

and

$$\mathbf{F} = \begin{bmatrix} \mathbf{F}_{31} & \mathbf{F}_{31} & \mathbf{F}_{31} \\ \mathbf{F}_{12} & \mathbf{F}_{12} & \mathbf{F}_{12} \\ & & \\ \mathbf{F}_{12} & \mathbf{F}_{12} & \mathbf{F}_{12} \\ \mathbf{F}_{23} & \mathbf{F}_{23} & \mathbf{F}_{23} \\ & & \\ \mathbf{F}_{23} & \mathbf{F}_{23} & \mathbf{F}_{23} \\ \mathbf{F}_{31} & \mathbf{F}_{31} & \mathbf{F}_{31} \end{bmatrix} \quad \text{where} \quad \begin{aligned} \mathbf{F}_{12} &= \begin{bmatrix} \frac{1}{l_{12}^2} & \frac{n_{12x}}{l_{12}} & \frac{n_{12y}}{l_{12}} \end{bmatrix} \\ \mathbf{F}_{23} &= \begin{bmatrix} \frac{1}{l_{23}^2} & \frac{n_{23x}}{l_{23}} & \frac{n_{23y}}{l_{23}} \end{bmatrix} . \\ \mathbf{F}_{31} &= \begin{bmatrix} \frac{1}{l_{31}^2} & \frac{n_{31x}}{l_{31}} & \frac{n_{31y}}{l_{31}} \end{bmatrix} \end{aligned} \tag{4.4.5}$$

The six curvature gage readings in $\mathbf{g}$ give two curvature gage readings at each node. But three natural coordinate curvature readings are necessary to transform to the Cartesian strains at each node. A third reading is obtained by invoking the following *projection rule* [00]: the natural curvature κ_{ij} is assumed to vary linearly along side ij and constant along lines normal to side ij. Node k is then assigned a κ_{ij} value according to the projection of the node on line ij. This assumption can be expressed as the matrix relationship

$$\boldsymbol{\kappa} = \mathbf{A}_\kappa \mathbf{g} \ , \tag{4.4.6}$$

where

$$\mathbf{A}_\kappa = \tag{4.4.7}$$

$$\begin{bmatrix} 0 & \zeta_1 + \lambda_{12}\zeta_3 & \zeta_1 + \lambda_{21}\zeta_3 & 0 & 0 & 0 \\ 0 & 0 & 0 & \zeta_2 + \lambda_{23}\zeta_1 & \zeta_2 + \lambda_{32}\zeta_1 & 0 \\ \zeta_1 + \lambda_{13}\zeta_2 & 0 & 0 & 0 & 0 & \zeta_3 + \lambda_{31}\zeta_2 \end{bmatrix}$$

and

$$\lambda_{ij} = \frac{-\mathbf{s}_{ki}^T \mathbf{s}_{ij} l_{ki}}{l_{ij}} \ .$$

The deviatoric parts of the strains are now obtained by subtracting the mean strain:

$$\mathbf{A}_{\kappa d} = \mathbf{A}_\kappa - \int_A \mathbf{A}_\kappa \, dA \ ,$$

which gives

$$\mathbf{A}_{\kappa d} = \tag{4.4.8}$$

$$\begin{bmatrix} 0 & \tilde{\zeta}_1 + \lambda_{12}\tilde{\zeta}_3 & \tilde{\zeta}_1 + \lambda_{21}\tilde{\zeta}_3 & 0 & 0 & 0 \\ 0 & 0 & 0 & \tilde{\zeta}_2 + \lambda_{23}\tilde{\zeta}_1 & \tilde{\zeta}_2 + \lambda_{32}\tilde{\zeta}_1 & 0 \\ \tilde{\zeta}_1 + \lambda_{13}\tilde{\zeta}_2 & 0 & 0 & 0 & 0 & \tilde{\zeta}_3 + \lambda_{31}\tilde{\zeta}_2 \end{bmatrix}$$

in which $\tilde{\zeta}_i = \zeta_i - \frac{1}{3}$.

The deviatoric cartesian curvatures.
The deviatoric cartesian strain distribution over the element can now be expressed as

$$\kappa_d = \mathbf{T}\boldsymbol{\kappa} = \mathbf{T}\mathbf{A}_{\kappa d}\mathbf{g} = \mathbf{T}\mathbf{A}_{\kappa d}\mathbf{Q}\mathbf{v} = \mathbf{B}_d\mathbf{v} \ ,$$

where $\mathbf{T}$ is defined in equation (4.3.15).

The higher order stiffness.
Finally, the higher order stiffness can be computed from the deviatoric strains as

$$\mathbf{K}_h = \int_A \mathbf{B}_d^T \mathbf{C}\mathbf{B}_d \ dA \ . \tag{4.4.9}$$

4.5 Nonlinear extensions for a triangular shell element.

The linear triangular shell element is now ready to be incorporated in the co-rotational formulation discussed in Chapter 2. The shadow element C_{0n} is best fit to the deformed element C_n by a rigid body motion of the undeformed initial element C_0. However this "best fit" is not unique. The rotation gradient matrix $\mathbf{G}$ defined in equation (0.0.0) can be split into contributions from each node as

$$\delta\tilde{\boldsymbol{\omega}}_r = \tilde{\mathbf{G}}\,\delta\tilde{\mathbf{v}} \quad \text{where} \quad \tilde{\mathbf{G}} = [\,\tilde{\mathbf{G}}_1 \quad \tilde{\mathbf{G}}_2 \quad \tilde{\mathbf{G}}_3\,] = \begin{bmatrix} \tilde{\mathbf{G}}_{\theta_x} \\ \tilde{\mathbf{G}}_{\theta_y} \\ \tilde{\mathbf{G}}_{\theta_z} \end{bmatrix}, \tag{4.5.1}$$

and $\delta\tilde{\mathbf{v}}$ is defined as

$$\delta\tilde{\mathbf{v}} = \begin{Bmatrix} \delta\tilde{\mathbf{v}}_1 \\ \delta\tilde{\mathbf{v}}_2 \\ \delta\tilde{\mathbf{v}}_3 \end{Bmatrix} \quad \text{where} \quad \delta\tilde{\mathbf{v}}_i = \begin{Bmatrix} \delta\tilde{\mathbf{u}}_i \\ \delta\tilde{\boldsymbol{\omega}}_i \end{Bmatrix}. \tag{4.5.2}$$

Three techniques for fitting the shadow element are discussed below. Each technique produces different $\tilde{\mathbf{G}}_i$ submatrices.

4.5.1 Aligning a triangle side.

This procedure is similar to Rankin's alignment of the C_{0n} and C_n elements [00] in that it uses a common side edge direction for those configurations. Whereas Rankin picks side 13 for the unit-vector $\mathbf{e}_2$ and node 1 as the origin of the coordinate system, the current approach aligns the directions of side 12 with the $\mathbf{e}_1$ axis and uses the element nodal average (triangle centroid) as the origin of the coordinate system. This choice of centroid as origin is necessary in order to satisfy the orthogonality of $\mathbf{P}_T$ and $\mathbf{P}$ in equation (0.0.0) .

Through consistent variation of the foregoing choice of local coordinate system, the nodal submatrices $\tilde{\mathbf{G}}_i$ of equation (4.5.1) is obtained as

$$\begin{aligned}
\tilde{\mathbf{G}}_1 &= \frac{1}{2A}\begin{bmatrix} 0 & 0 & x_{32} & 0 & 0 & 0 \\ 0 & 0 & y_{32} & 0 & 0 & 0 \\ 0 & -\frac{2A}{l_{12}} & 0 & 0 & 0 & 0 \end{bmatrix}, \\
\tilde{\mathbf{G}}_2 &= \frac{1}{2A}\begin{bmatrix} 0 & 0 & x_{13} & 0 & 0 & 0 \\ 0 & 0 & y_{13} & 0 & 0 & 0 \\ 0 & \frac{2A}{l_{12}} & 0 & 0 & 0 & 0 \end{bmatrix}, \\
\tilde{\mathbf{G}}_3 &= \frac{1}{2A}\begin{bmatrix} 0 & 0 & x_{32} & 0 & 0 & 0 \\ 0 & 0 & y_{32} & 0 & 0 & 0 \\ 0 & 0 & 0 & 0 & 0 & 0 \end{bmatrix},
\end{aligned} \tag{4.5.3}$$

where A is the area of the triangle and l_{12} is length of side 12. (This variation is carried out in more detail for the four node shell element i Section 0.0.)

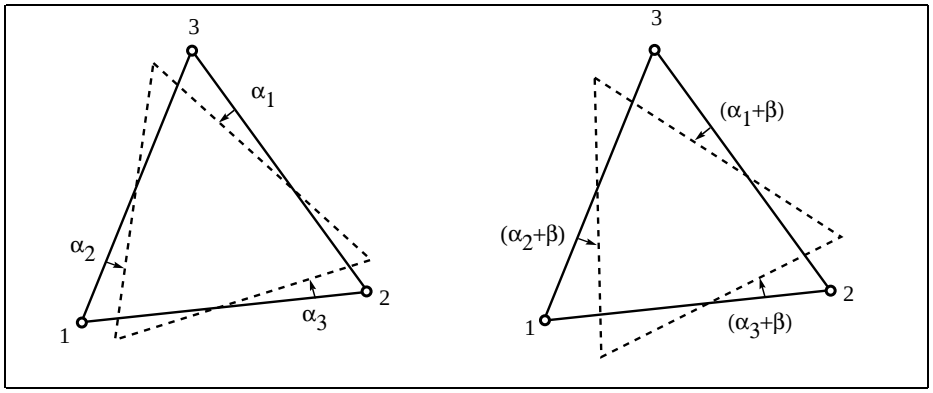

Figure 4.2. Definition of side edge angular errors.

The in-plane rotations can be recognized as $\omega_x = \frac{\partial w}{\partial y}$ and $\omega_y = -\frac{\partial w}{\partial x}$, using the geometric shape functions to interpolate w. This choice of shadow element fit satisfies the required splitting of the rotation gradient matrix as $\tilde{\mathbf{G}} = \tilde{\mathbf{X}}\mathbf{A}$ where only matrix $\mathbf{X}$ is coordinate dependent as required for the consistency condition in equation (0.0.0). On the other hand, this choice does not give an invariant deformational displacement vector for the element in the sense discussed in Section 0.0.0.

4.5.2 Least square fit of side edge angular errors.

Nygård [00] and Bjærum [00] place the C_{0n} element in the plane of the deformed element C_n with node 1 coinciding. The present study utilizes coinciding centroids. The in-plane orientation of the shadow element is then determined by a least square fit of the side edge angular errors. According to Figure 4.2 the squared-error sum is

$$e^2 = \alpha_1^2 + \alpha_2^2 + \alpha_3^2 \, . \tag{4.5.4}$$

By rotating the shadow element an angle β the square of the errors becomes

$$e^2(\beta) = (\alpha_1 + \beta)^2 + (\alpha_2 + \beta)^2 + (\alpha_3 + \beta)^2 \, . \tag{4.5.5}$$

Minimizing with respect to β:

$$\frac{\partial e^2(\beta)}{\partial \beta} = 0 \quad \Rightarrow \quad \beta = -\frac{1}{3}(\alpha_1 + \alpha_2 + \alpha 3) \, . \tag{4.5.6}$$

Consequently, the optimal in-plane position of the shadow element according to this algorithm is given by the mean of the side edge angular errors. This condition yields for the nodal submatrices

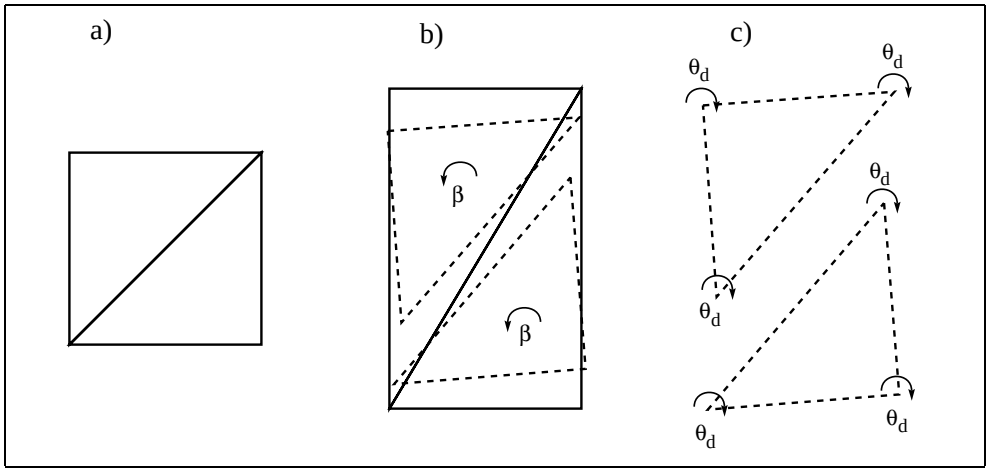

Figure 4.3. Patch of triangle elements subjected to pure stretching.

$$\tilde{\mathbf{G}}_i = \frac{1}{2A}\begin{bmatrix} 0 & 0 & x_{kj} & 0 & 0 & 0 \\ 0 & 0 & y_{kj} & 0 & 0 & 0 \\ \frac{2A}{3}(-\frac{s_{jy}}{l_j}+\frac{s_{ky}}{l_k}) & \frac{2A}{3}(\frac{s_{jx}}{l_j}-\frac{s_{kx}}{l_k}) & 0 & 0 & 0 & 0 \end{bmatrix}. \qquad (4.5.7)$$

The major advantage of this method is that it gives a unique fit independent of node numbering, which leads to a invariant deformational displacement vector as discussed in section 0.0.0. The rotational gradient matrix cannot be split into a coordinate dependent and independent part in order to be consistent with equation (0.0.0). However, again, this is of minor importance for triangular elements since the shadow element C_{0n} and the deformed element C_n will be close together for small membrane strains.

A more serious disadvantage of this fitting method is that it reintroduces the problem of fictitious normal rotations when an element is subjected to pure stretch.

This difficulty is illustrated in Figure 4.3, where the C_{0n} elements rotate due to the in-plane rotation of the diagonal. The deformational displacement vector is then computed as the difference between C_n and C_{0n}. A deformational normal rotation is thus picked up since the predictor step gives no rotation at the nodes and the deformational rotation is the total rotation minus the rigid body rotation

$$\theta_d = (\theta - \beta) = -\beta\ . \qquad (4.5.8)$$

This problem is similar to that pointed out by Irons and Ahmad [00] when defining drilling degrees of freedom as the mean of the side edge rotations at an

node. This was overcome by Bergan and Felippa [00] when they defined the normal rotation as $\theta_z = \frac{1}{2}(\frac{\partial v}{\partial x} - \frac{\partial u}{\partial y})$ for the linear FF membrane element. It is seen that the problem of fictitious normal rotations has been thus been re-introduced for the nonlinear case by the choice of shadow element positioning. This problem is even more pronounced with the side edge alignment procedure described in Section 4.5.1.

4.5.3 Fit according to CST-rotation.

As with the least square fit of side edge angular errors the shadow C_{0n} element is chosen to be co-planar with the deformed element C_n, and the centroids coincide.

By using the normal rotation of the CST element as the rigid body rotation β for the in-plane positioning of the shadow element, one avoids the problem of fictitious normal rotations when an element is subjected to pure stretching.

The definition $\theta_z = \frac{1}{2}(\frac{\partial v}{\partial x} - \frac{\partial u}{\partial y})$ gives an invariant definition of the normal rotation for the infinitesimal case. This also provides the variation of the rigid body rotation with respect to the visible degrees of freedom.

Extending the above definition to finite rotations seems to suggest

$$\theta_z = \frac{1}{2}(\tan^{-1}(\frac{\Delta v}{\Delta x}) - \tan^{-1}(\frac{\Delta u}{\Delta y})) \; . \tag{4.5.9}$$

However this choice gives slightly varying results with respect to the orientation of the (x, y)-coordinate system. In order to obtain a completely invariant positioning with respect to node numbering, the rigid body rotation can been computed as the average of the rotations obtained with the local x-axis along each of the three side edges. The continuum mechanics definition of the normal rotation is $\tilde{\theta}_z = \frac{1}{2}(\frac{\partial v}{\partial x} - \frac{\partial v}{\partial x})$. This definition is invariant with respect to the orientation of the x and y coordinate axis, and gives the rotation gradient matrix as

$$\tilde{\mathbf{G}}_i = \frac{1}{2A}\begin{bmatrix} 0 & 0 & x_{kj} & 0 & 0 & 0 \\ 0 & 0 & y_{kj} & 0 & 0 & 0 \\ -\frac{1}{2}x_{kj} & -\frac{1}{2}y_{kj} & 0 & 0 & 0 & 0 \end{bmatrix} \tag{4.5.10}$$

In the present investigation the three techniques just outlined for choosing the shadow element position were tested in the nonlinear problems reported in Chapters 7 and 8.